Open camera or QR reader and
scan code to access this article
and other resources online.

How Habitable Are M Dwarf Exoplanets? Modeling Surface Conditions and Exploring the Role of Melanins in the Survival of *Aspergillus niger* Spores Under Exoplanet-Like Radiation

Afonso Mota,[1,2] Stella Koch,[1] Daniel Matthiae,[3] Nuno Santos,[2,4] and Marta Cortesão[1]

Abstract

Exoplanet habitability remains a challenging field due to the large distances separating Earth from other stars. Using insights from biology and astrophysics, we studied the habitability of M dwarf exoplanets by modeling their surface temperature and flare ultraviolet (UV) and X-ray doses using the martian atmosphere as a shielding model. Analyzing the Proxima Centauri and TRAPPIST-1 systems, our models suggest that Proxima b and TRAPPIST-1 e are likeliest to have temperatures compatible with surface liquid water, as well as tolerable radiation environments. Results of the modeling were used as a basis for microbiology experiments to assess spore survival and germination of the melanin-rich fungus *Aspergillus niger* to exoplanet-like radiation (UV-C and X-rays). Results showed that *A. niger* spores can endure superflare events on M dwarf planets when shielded by a Mars-like atmosphere or by a thin layer of soil or water. Melanin-deficient spores suspended in a melanin-rich solution showed higher survival rates and germination efficiency when compared to melanin-free solutions. Overall, the models developed in this work establish a framework for microbiological research in habitability studies. Finally, we showed that *A. niger* spores can survive harsh radiation conditions of simulated exoplanets, which also emphasizes the importance of multifunctional molecules like melanins in radiation shielding beyond Earth. Key Words: Exoplanets—M dwarfs—Radiation—*Aspergillus niger*—Habitability—Melanin. Astrobiology 25, 161–176.

1. Introduction

Conventionally, exoplanet habitability is assessed solely by the planet's orbital distance to its star and whether that orbit is present within the star's expected "Goldilocks" or "habitable" zone (Kasting et al., 1993). However, this is a reductionistic description of habitability—not only does it depend on many other factors, but the definition focuses only on Earth-like planets, leaving out cases where planets and moons outside this zone may harbor habitable conditions, both in our solar system (Nimmo and Pappalardo,

2016) and beyond (Madhusudhan et al., 2021; Seager, 2013).

Exoplanets are notoriously difficult to observe and study due to the large distances that separate Earth from even the closest stars. That said, developments have been made toward the identification of rocky planets orbiting M dwarf stars, the smallest, coolest, and most common stars in the Universe. Future studies will be able to characterize exoplanet atmospheres, and this is considered one of the main avenues for the possible detection of potential biosignatures (Palle et al., 2023). Moreover, telescope technology and data

---

[1]Aerospace Microbiology Research Group, Institute of Aerospace Medicine, German Aerospace Center (DLR), Cologne, Germany.
[2]Instituto de Astrofísica e Ciências do Espaço, Universidade do Porto, CAUP, Porto, Portugal.
[3]Biophysics Research Group, Institute of Aerospace Medicine, German Aerospace Center (DLR), Cologne, Germany.
[4]Departamento de Física e Astronomia, Faculdade de Ciências, Universidade do Porto, Porto, Portugal.

analysis techniques are continuously improving. In the next few years, many more planets will be revealed in the Milky Way, some of which could have habitable conditions where we may be able to find indications of the presence of life (Rauer et al., 2014). Presently, there is a need to build interdisciplinary tools and experiment pipelines that allow astrobiologists to use current and novel information to perform more detailed analyses of the potential survival and growth of organisms on exoplanets.

The study of exoplanet habitability is a critical aspect of astrobiology, as it provides insights into the potential existence of life outside of Earth, within and beyond our solar system. Both the planet's surface temperature and radiation environment play a crucial role in determining habitability. Ultraviolet (UV) radiation and X-rays can be detrimental to potential organisms on the surface, as well as alter a planet's atmospheric composition, particularly for planets orbiting M dwarf stars, which have increased activity and strong flares (Howard et al., 2018; Tilley et al., 2019; Yamashiki et al., 2019).

The study of microbial extremophiles is particularly relevant in astrobiology, as it can provide information about the potential for life in extraterrestrial environments that may resemble these extreme conditions on Earth (*e.g.*, Brock et al., 2003; Cortesão et al., 2020; Pacelli et al., 2020). Within the microbial world, pigments are a diverse group of compounds that contribute to the survival of many extremophiles and exhibit a remarkable range of colors, structures, and functions. These serve various roles in cellular processes such as thermoregulation, quenching oxidative stress, and cellular messaging (Malik et al., 2012). Pigments have been proposed as promising biosignatures for exoplanets (Coelho et al., 2022; Schwieterman et al., 2015). Melanins, in particular, are found in both eukaryotic and prokaryotic microorganisms, where they enhance survival in extreme environments (Cordero and Casadevall, 2017). It has been proposed that melanins or similar pigments could have been key for the origin and development of life on Earth (d'Ischia et al., 2021) and perhaps on other worlds.

In the context of astrobiology, and particularly astromycology, the study of extremotolerant fungi has proven critical to better understanding the limits of life and habitability. The field has advanced significantly through experiments such as LIFE (Onofri et al., 2015) and the subsequent BIOMEX experiment (de Vera et al., 2019). *Aspergillus niger*, an extremotolerant filamentous fungus, has been frequently used as a model organism to study fungal survival in extreme environments, as it grows in a wide range of conditions (Cortesão et al., 2020). *A. niger* spores have a dense and complex melanin coating, which increases their resistance to many stresses, such as UV and X-ray radiation and oxidative stress (Cortesão et al., 2020; Xu et al., 2022). *A. niger* has also been found to be present in space stations, which highlights its endurance to the conditions of space (Cortesão et al., 2021; Romsdahl et al., 2018). Furthermore, *A. niger* has been extensively studied as a model organism for biotechnology and microbiology (Cairns et al., 2018). A key question is whether these spores can not only endure high radiation environments but also reenter a metabolically active state. This is crucial when considering environments subjected to strong stellar flares, where more vulnerable structures like mycelium might not survive. In such scenarios, spores could persist, which would allow the population to quickly regrow.

This study adopted an interdisciplinary approach that bridges astrophysics and microbiology to explore what might constitute a habitable M dwarf exoplanet by

- Developing models for estimating the surface temperature of rocky exoplanets, as well as their radiation environment. For radiation modeling, Mars-like atmospheric properties were used, due to the red planet's high astrobiological relevance and proposed indications of potential past or present habitability.
- Assessing potential survivability by exposing the model fungus *A. niger* spores to the most harmful electromagnetic radiation produced during M dwarf flares (UV and X-rays).
- Determining *A. niger* spore's ability to reenter a metabolically active state after exoplanet-like radiation exposure and examining the role of solubilized melanin in enhancing spore resistance and germination.

Thus, in our study, we present how *A. niger* spore resistance and germination serve as a proxy for habitability by indicating how life may recover and maintain biological processes after exoplanet-like extreme events.

2. Materials and Methods

2.1. Selection of exoplanet systems and planetary parameters

To provide a testbed for exoplanet habitability, this work focused on two astrobiologically relevant star systems— Proxima Centauri (referred to hereafter simply as Proxima) and TRAPPIST-1. The studied rocky exoplanets were Proxima b and d, and TRAPPIST-1 d, e, and f. Proxima b is thought to be a somewhat cool Earth-like planet with a tidally locked or 3:2 resonant orbit (Anglada-Escudé et al., 2016; Boutle et al., 2017; Sergeev et al., 2020; Suárez Mascareño et al., 2020; Turbet et al., 2016). Proxima d is a small sub-Earth discovered in 2022, which is likely dry and barren (Faria et al., 2022). TRAPPIST-1 d, e, and f are inside their star's optimistic "Goldilocks" zone. TRAPPIST-1 e is thought to be one of the exoplanets found so far that is most likely to have habitable conditions (Krissansen-Totton and Fortney, 2022; Quarles et al., 2017; Sergeev et al., 2020). Finally, TRAPPIST-1 f has an Earth-like mass and radius (Agol et al., 2021). Although previous research suggested it may have limited habitability due to a massive water-rich envelope with surface temperature and pressure too high for liquid water (Quarles et al., 2017), recent findings have indicated that it may have a cold but habitable climate, perhaps with liquid water on its surface (Krissansen-Totton and Fortney, 2022). Table 1 shows the relevant planetary parameters used in this study, with the solar system's rocky planets included as examples. Stellar temperatures (Agol et al., 2021; Pavlenko et al., 2017; Williams, 2022) and planet semimajor axes (Agol et al., 2021; Faria et al., 2022; Williams, 2023) were taken from the literature and used to calculate the incident flux for each exoplanet.

2.2. Modeling of exoplanet conditions

2.2.1. *Estimating rocky planet surface temperatures.* A crucial factor that controls habitability is the planet's surface temperature, which is difficult to determine since it is

Planet	Semimajor axis (AU)	Incident flux (W/m²)
Mercury	0.387	9088
Venus	0.723	2604
Earth	1.000	1361
Mars	1.524	589
Proxima d	0.02886	2476 ± 31
Proxima b	0.04858	874 ± 10
TRAPPIST-1 d	0.02227	1523 ± 26
TRAPPIST-1 e	0.02925	883 ± 15
TRAPPIST-1 f	0.03849	510 ± 9

Incident flux is calculated as $F = (\sigma R_\star{}^2 T_\star{}^4)/a^2$, where $T_\star$ and $R_\star$ are the star's temperature and radius (Agol et al., 2021; Pavlenko et al., 2017; Williams, 2022), respectively, and a is the planet's semimajor axis (Agol et al., 2021; Faria et al., 2022; Williams, 2023). σ is the Stefan–Boltzmann constant.

influenced by many factors, such as albedo and greenhouse effect (Seager, 2011; Sergeev et al., 2020). However, for exoplanets, most of these factors are not easily known. Therefore, a more commonly used model is equilibrium temperature (T_{eq}), a theoretical temperature value that follows several assumptions such as the absence of an atmosphere and a perfect heat distribution (Kump et al., 2014). Naturally, this is not necessarily a good representation of the surface temperature of the planet, and complex models are frequently employed to study possible scenarios and the corresponding surface temperature distributions (*e.g.*, Boutle et al., 2017). However, a simple model remains to be developed that considers factors such as atmospheric greenhouse effect, energy distribution efficiency, and planetary reflectivity (albedo) without requiring the detailed knowledge that most climate models need (*e.g.*, Godolt et al., 2016; Lincowski et al., 2018), but still produces accurate general predictions when compared to the equilibrium temperature.

We developed a simple equation based on the T_{eq} that can be employed to better estimate the surface temperature of rocky exoplanets, which depends upon several factors. First, we considered a factor ε representing the atmospheric greenhouse effect, variable between 0 (no greenhouse, *e.g.*, Mercury) and 1 (strong greenhouse, *e.g.*, Venus), as well as N, the number of simulated atmospheric layers. Earth has an ε value of 0.77–0.79 (Jacob, 1999; Liu, 2020). For very powerful greenhouses, such as Venus-like planets, $N \gg 1$, while for all other cases, $N = 1$ (Liu, 2020). To account for orbital resonance patterns, such as tidal locking, we added a variable f ($0.5 < f < 1$) that represents the energy distribution efficiency of a planet, as proposed in previous research (Seager, 2011). In tidally locked planets with no energy redistribution, $f = 0.5$. For planets with efficient heat diffusion, $f = 1$. A final model equation for the dayside temperature can be written as follows:

$$T_d = \sqrt[4]{\frac{N \cdot F(1 - A_B)}{4f\sigma\left(1 - \frac{\varepsilon}{2}\right)}} = T_{eq} \cdot \sqrt[4]{\frac{N}{f\left(1 - \frac{\varepsilon}{2}\right)}} \quad (1)$$

F is the energy flux that reaches the planet, σ is the Stefan–Boltzmann constant, and A_B is the Bond albedo of the planet is used to calculate the T_{eq}. A more detailed description of the derivation process can be found in the Supplementary Data S1.

2.2.2. X-ray fluxes at the top-of-atmosphere of M dwarf exoplanets.

A stellar flare is a sudden and dramatic increase in a star's brightness caused by a large-scale magnetic event, which releases a substantial amount of energy across the electromagnetic spectrum, including X-rays and UV light. The average expected X-ray energy released during a standard M dwarf flare is around 2.5×10^{30} erg (Welsh et al., 2007). We considered this value when simulating an average flare from Proxima; however, since TRAPPIST-1 produces generally less energetic flares (Maas et al., 2022; Yamashiki et al., 2019), we assume a mean of 1.0×10^{30} erg of X-rays released by a conventional flare. Hence, the total estimated energy per unit area that reaches a certain planet's top-of-atmosphere (TOA) can be calculated by using the inverse-square law applied to its orbital semimajor axis (a):

$$E_p \left(\frac{J}{m^2}\right) = E_{flare}(erg) \times 10^{-7} \times \frac{1}{4\pi a^2} \quad (2)$$

Here, the 10^{-7} factor serves to convert the flare energy from ergs to joules, as flare energies are traditionally presented in erg. Although spectra of the X-ray photon energy distributions of M dwarf stellar flares have not yet been acquired (to the best of our knowledge), it is expected that these will follow a power law, similar to the Sun's X-ray emission during a flare. The Sun's X-ray photon output (1–100 keV) during observed flares has been compiled in previous studies, such as those by Maggio (2008) and Inglis (2009). Regression analysis of both sets of data was performed and used to fit power law equations to model the photon release during flares (Fig. 1).

To create a general model for an average flare, we took the mean of the exponents from both equations, getting $k = -3.4845$. Hence, the best-fit equation to calculate the stellar photon fluence in the X-ray wavelength range (1–100 keV) is as follows:

$$F(E) = F_1 \times E^{-3.4845} \quad (3)$$

Here, E is the photon energy (in keV), and F_1 represents the initial condition of the power law, that is, the absolute flux of photons with $E = 1$ keV. Therefore, F_1 is variable depending on the considered flare energy, and its value is larger for stronger flares. The total X-ray energy received by a planet during a flare, E_p, can be calculated by considering the stellar X-ray photon fluence $F(E)$, determined in Equation 3, as an integration within the X-ray energy wavelengths (E, from 1 to 100 keV):

$$E_p = \int_1^{100} E \times F(E) \, dE \quad (4)$$

When integrated numerically and rearranged, this equation gives the X-ray photon fluence on the planet, $\theta(E)$, in photons/(m^{-2} keV^{-1}), as follows:

$$\theta(E) = 1.4022 \times E_p \times E^{-3.4845} \quad (5)$$

The $\theta(E)$ represents the number of photons for each energy value and therefore is useful to calculate the dose throughout the X-ray wavelengths. X-rays are measured in absorbed dose (Gy, J/kg), and the same X-ray flux can lead

Modelled flare X-ray photon fluence
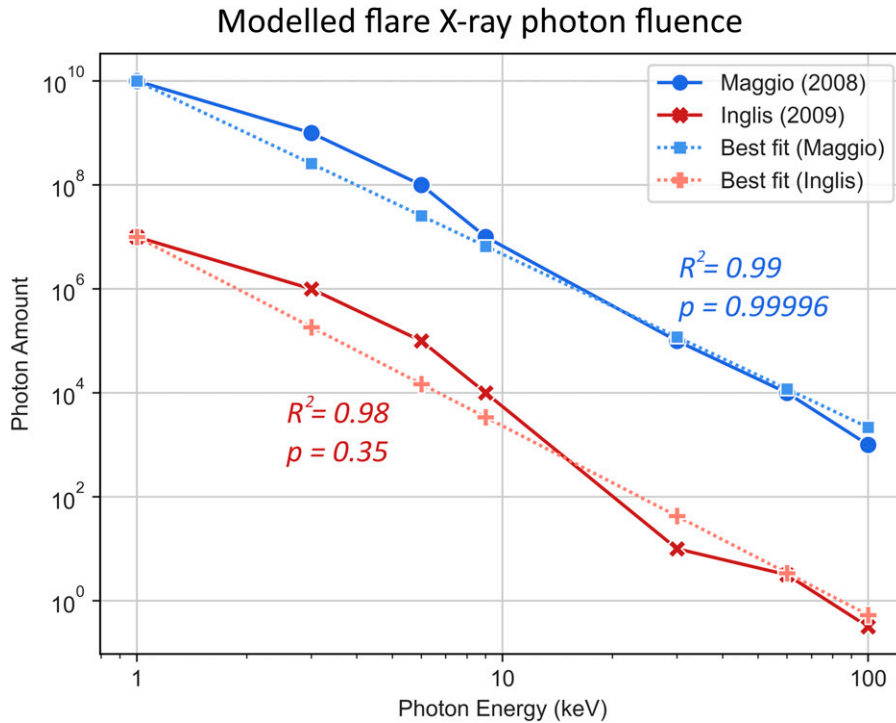
FIG. 1. Photon fluence (photons/[cm²·keV]) in the X-ray band during an average solar flare as shown in Maggio (2008), over 100 s, and Inglis (2009) over 1 s. *p*-Values shown are from Kolmogorov–Smirnov tests and indicate that the fit equations are adequate representations of the data.

to different absorbed doses based on the irradiated material. Conversion from energy flux to absorbed dose is not direct, but an estimation can be done using the target's mass-energy absorption coefficient ($\frac{\mu_{en}}{\rho}$) (Hubbell and Stephen, 1995). The most accurate materials to use as a reference to microbes are liquid water and soft tissue (ICRU-44), with similar $\frac{\mu_{en}}{\rho}$.

Assuming an approximately constant fluence over the target volume, the absorbed dose ($D(E)$) for photons of energy E can be calculated with the previously described $\frac{\mu_{en}}{\rho}$ values, without attenuation, using the following factor δ:

$$\delta(E) = E \cdot \frac{\mu_{en}}{\rho}(E) \cdot \theta(E) \qquad (6)$$

However, since $\frac{\mu_{en}}{\rho}$ data come from discrete data points, we must consider the distance between tabled energy values (ΔE_i) in the calculations, as well as the average $\delta(E)$ between successive data points. Therefore, the equation for determining $D(E)$ emerges as follows:

$$D(E) = (E_{i+1} - E_i) \cdot \frac{\delta(E_i) + \delta(E_{i+1})}{2} \qquad (7)$$

Equation 7 yields the dose values in keV/kg. This result can then be converted to J/kg.

2.2.2.1. Atmospheric attenuation of X-rays and (sub)surface doses.
Additionally, to model the physical attenuation of X-rays passing through a planet's atmosphere, surface, or water layers, we used Mars as a model planet for its astrobiological relevance, taking compositions of martian soil simulant (MGS-1) from literature (Cannon et al., 2019) and assuming an atmospheric content 95% CO_2 and 5% N_2. The interaction of X-rays with the martian atmosphere has been previously modeled (Smith and Scalo, 2007), from which we calculated the fraction of transmitted photons over

several wavelengths by dividing the surface photon amount by the incident photon amount at the TOA. These values are plotted in Figure 2. Then, through least squares fitting, we obtained the equation for the atmospheric transmission fraction (T_A) over the X-ray wavelengths (1–100 keV), which follows the function $T_A(E) = \frac{0.2579}{1 + e^{-0.1102 \cdot (E - 41.54)}} - 0.0194$ (Fig. 2). For surface attenuation (water and Mars-like soil), mass attenuation ($\frac{\mu}{\rho}$; Berger, 1998) values were used. X-ray transmittance through a material follows the law $T_S(E) = e^{-\frac{\mu}{\rho}(E) \cdot x \cdot \rho}$, where x is the depth traversed by the photons, and ρ the material density—1000 kg/m³ for water and 1290 kg/m³ for martian soil (Cannon et al., 2019)—which results in an estimation of the surface attenuation (T_S).

Factoring in both T_A and T_S yields a final model for estimating the surface or subsurface X-ray absorbed dose of a Mars-like model exoplanet:

$$\hat{D}(E) = D(E) \cdot T_A(E) \cdot T_S(E) \qquad (8)$$

2.2.3. UV fluxes at the TOA and surface of M dwarf exoplanets.
M dwarf flare energies in the UV range are similar to the X-ray fluxes (Welsh et al., 2007). However, unlike for X-rays, the UV flux of M dwarfs during flares tends to be similar across the UV wavelength range, with only a slight increase from lower to higher wavelengths (Ranjan et al., 2017; Segura et al., 2010; Tilley et al., 2019). Therefore, for this work, we assumed a constant flux across the UV range for flares of Proxima Centauri and TRAPPIST-1. Furthermore, the UV spectrum is divided into UV-A (315–400 nm), UV-B (280–315 nm), and UV-C (100–280 nm), where UV-C is the most harmful (Bucheli-Witschel et al., 2010). Since the UV flux is uniform across wavelengths, the estimated fractions of each UV type are 28.3% UV-A, 11.7% UV-B, and 60.0% UV-C.

FIG. 2. Modeled X-ray transmittance of the martian atmosphere based on data from Smith and Scalo (2007). The data points taken were those for a stronger flare (spectral index $p = 2.5$) at an atmospheric column density of 16 g/cm^2. As shown in the figure, the Kolmogorov–Smirnov test ($p = 1.0$) indicates that the fitted curve is an adequate model of the data.
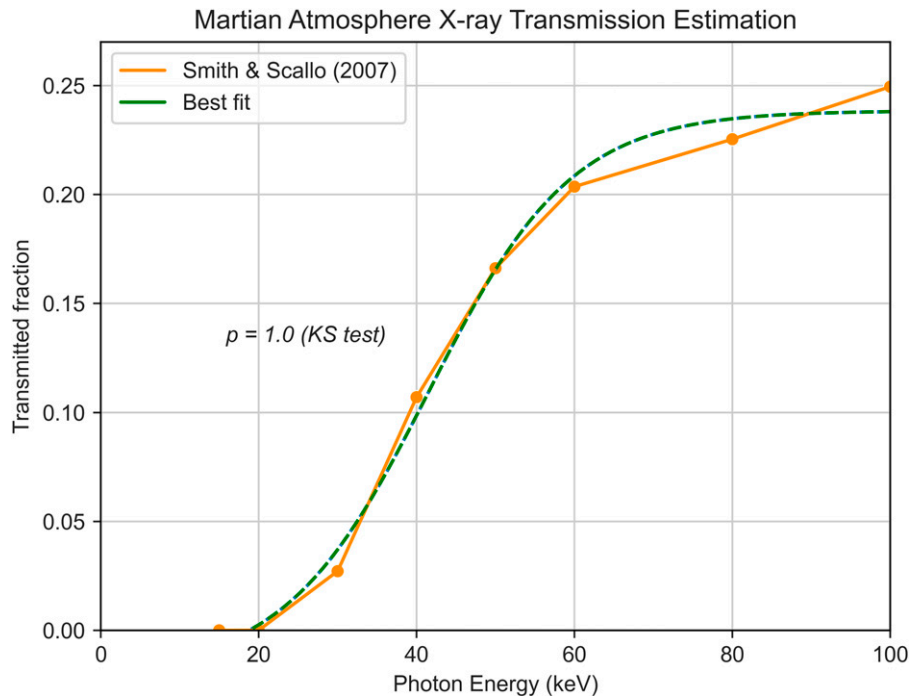
We modeled the UV attenuation by the martian atmosphere by using data from Cockell et al. (2000) (Fig. 3). UV light below 200 nm is completely attenuated by the martian atmosphere.

2.3. Estimating the survival of model organisms to the calculated radiation doses

After calculating the surface UV and X-ray dose for each planet using the modeled transmittance curves, we compared these results to the LD$_{90}$ (D$_{10}$) values—the radiation dose required to kill 90% of a population of a certain microorganism—of three model microbes. The selected organisms were *Escherichia coli* (mesophile), *A. niger* (extremotolerant, high UV resistance), and *Deinococcus radiodurans* (polyextremophile, high X-ray resistance). *Escherichia coli* LD$_{90}$ values are 22.6 J/m^2 for UV (Gascón et al., 1995) and 200 Gy for X-rays (Moreira et al., 2012). *A. niger* LD$_{90}$ values are 1038 J/m^2 for UV and 366 Gy for X-rays (Cortesão et al., 2020). *Deinococcus radiodurans* LD$_{90}$ values are 533 J/m^2 for UV (Gascón et al., 1995) and 1.6×10^4 Gy for X-rays (Slade

FIG. 3. Dots and straight lines represent the martian atmosphere's UV transmission fraction calculated from Cockell et al. (2000). Maximum transmission conditions involve clear skies (little suspended dust) and vertical photon flux (shorter atmospheric interaction distance); intermediate conditions are clear skies with light rays hitting the planet at a 60° angle; minimum transmission comprises a dusty atmosphere and 60° ray angle. Dashed lines are calculated curves fitting the data with corresponding Pearson's correlation values (R^2). UV, ultraviolet.
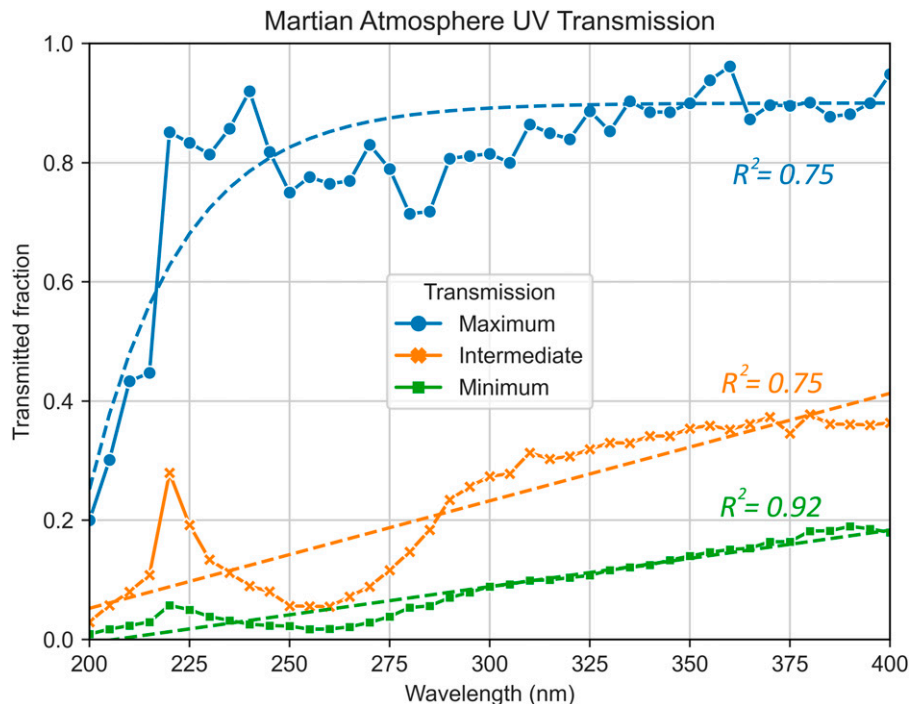
and Radman, 2011). LD$_{90}$ values were selected not to identify a total lethal dose threshold but as a measure to estimate general flare survivability for organisms with different susceptibilities to radiation exposure, both on the surface and subsurface of the studied exoplanets.

2.4. Experimental setup: Organisms, media, pigments

After models were created for studying rocky exoplanets, several microbiology experiments were conducted to test how fungal spores may endure exoplanet-like radiation. Three strains of *A. niger* were used in this work: a wild-type strain, N402; a DHN-melanin-deficient mutant strain, MA93.1 (Cortesão et al., 2020; Jørgensen et al., 2011); and a mutant strain modified to produce and excrete pyomelanin, OS4.3 (Koch et al., 2023). Spores were collected from 3-day-old cultures grown in complete medium (CM), prepared as shown in the work of Cortesão et al. (2020) at 30°C. After this, radiation exposure and viability assays were carried out using a minimal medium (MM) as described by Koch et al. (2023). All experiments were conducted using three technical replicates per strain ($n = 3$).

2.4.1. Pyomelanin solution preparation.
The use of a melanin-rich solution in our study simulates potential early-Earth conditions where melanin-like polymers delivered through meteorite impacts could have provided protection against ionizing radiation, catalyzed biochemical reactions, and facilitated the accumulation and preservation of life's building blocks (d'Ischia et al., 2021). We aimed to test how extracellular melanin could protect early life forms before organisms developed the ability to synthesize it internally. The melanin production and solution extraction process was adapted from the work of Koch et al. (2023), after which the pyomelanin-rich supernatant was filtered through a sterile Miracloth filter to eliminate any remaining hyphal fragments. This filtered solution was then stored at 4°C until it was used to suspend the spores for irradiation experiments. As controls, we used the standard 0.9% NaCl saline solution, as well as a N402-derived supernatant produced similarly to the process described above.

2.4.2. Radiation exposure conditions.
For UV and X-ray exposure, exoplanet-like doses were obtained by employing the models developed during this study, as described in Sections 2.2.2 and 2.2.3. Experiments were conducted assuming two types of flare events for the considered M dwarfs, standard flares and superflares. The used UV doses were 1000, 2500, and 5000 J/m^2 in addition to nonirradiated controls. *A. niger* spore irradiation was done as described in the work of Cortesão et al. (2020).

For UV, spores were subjected to UV radiation in Petri dishes (100 × 15 mm). Each sample contained 15 mL of a suspension of 10^6 spores/mL in 0.9% NaCl saline solution. At this concentration, spores form a monolayer, and no additional protection is caused by a high cell density (>10^7 spores/mL for larger volumes). A UV lamp (VL-215-LC, Vilbert Lourmat, SN. 14 100595) with a monochromatic UV-C wavelength of 254 nm was used for the irradiation process. Exposure time was calculated as $t(s) = \frac{R \times 100}{d}$, where $R\,(J/m^2)$ is the desired total flux, and $d\,(\mu W/cm^2)$ is the

dosimeter's measurement of UV fluence. Magnetic stirrers were utilized to continuously mix the spore suspension during exposure, which prevented settling of the spores on the bottom and the resulting mutual shielding among them. Spore viability and growth capability were assayed as shown in 2.3.3.

For X-rays, *A. niger* spores were suspended in PCR tubes (Brand) containing 100 μL of 0.9% NaCl saline solution at a concentration of 10^7 spores/mL. A higher concentration was used when compared to UV irradiation due to the reduced volume of the spore suspension; this ensured the presence of a monolayer, and thus no spore-to-spore protection, even at a higher cell density. The RS225 X-ray device (Gulmay Medical Systems, Camberley, Surrey, UK) was used for irradiation. It was operated unfiltered at 200 kV and 15 mA and thus enabled high-dose exposure in a short period. The X-ray machine outputs photons on a spectrum up to >100 keV, with the largest peak at around 60 keV. The dose rate (in Gy/min) was determined using the UNIDOS webline and a TM30013 ionization chamber (PTW, Freiburg, Germany), which allowed the calculation of the correct exposure time to achieve the desired X-ray absorbed doses for the samples. The X-ray doses used were 100, 500, and 1000 Gy, in addition to nonirradiated controls. Exposure time was calculated as $t(min) = \frac{R}{d}$, where $R\,(Gy)$ is the desired absorbed dose, and $d\,(Gy/min)$ is the measured dose rate.

2.4.3. Survival and growth assays.
The survival and viability of *A. niger* spores were assessed by testing their ability to form colonies following exposure to the experimental conditions. Serial dilutions of irradiated spore samples were prepared up to 10^{-6} in a 96-well plate, with a total volume of 100 μL per well. To determine the number of colony-forming units (CFUs), 20 μL of each dilution was plated on 1/6 of a Petri dish containing MM agar supplemented with 0.05% Triton X-100 to reduce colony size and aid in counting. After a 2-day incubation at 30°C, colonies were counted, and the survival fraction ratio ($\frac{N}{N_0}$) was calculated. Here, N represents the CFU for treated samples, while N_0 is the CFU for the controls.

Additionally, spore survival and growth profiles were further assessed via live-cell imaging using the oCelloScope™ (BioSense Solutions ApS, Farum, Denmark; Koch et al., 2023). To prepare the samples for observation of germination and hyphal formation, spore samples were diluted to a concentration of 10^5 spores/mL and incubated in liquid MM at 22°C over a 48-h period, after which no significant growth was seen. The oCelloScope analyzed the changing fungal biomass over time for each well using the built-in Segmentation and Extraction of Surface Area (SESA) fungi algorithm normalized at 4 h after inoculation in the medium, determined as the necessary amount of time for settling of spores (without germination), dust, and other suspended particles.

To compare the growth profile results generated by the oCelloScope, the Mann–Whitney (M-W) and Kruskal–Wallis (K-W) tests were performed due to the nonparametric nature of the data. For survival fraction evaluations (parametric data), t tests were used. The assumed significance threshold value was $p = 0.05$. Plot design and statistical analyses were done in Python.

3. Results

3.1. Dayside surface temperatures

Running the model from Equation 1 for a selected planet yields a dayside surface temperature matrix, with the calculated temperature depending on the greenhouse effect strength, Bond albedo, and energy distribution efficiency. Temperature matrices for Proxima d, Proxima b, TRAPPIST-1 e, and TRAPPIST-1 f are shown in Figure 4. The colormap was normalized with a minimum value of 235 K (−38°C) and a maximum value of 340 K (67°C) since modeling shows that surface temperatures below 235 K or above 340 K cannot sustain liquid water under any circumstances (Godolt et al., 2016). A surface temperature between 273 and 313 K (0°C and 40°C) has been suggested as being ideal to maximize habitability (Godolt et al., 2016). Results for TRAPPIST-1 d are also shown in the Supplementary Data S1 (Supplementary Fig. S2) for a thick Venus-like atmosphere and for a Mars- or Earth-like atmosphere.

Our results suggest that Proxima b and TRAPPIST-1 e are the likeliest to have temperatures compatible with liquid water on their surface and with the persistence of habitable environments. Proxima d and TRAPPIST-1 f are likely to have too high and low dayside temperatures, respectively.

Computing the model for all rocky planets of the Proxima and TRAPPIST-1 systems, assuming approximate values for factors A_B, f, ε, and N based on current data yields the results shown in Table 2. Earth-like values for all factors were used for Proxima b, TRAPPIST-1 e, and TRAPPIST-1 f, except $f = 0.75$ (instead of 1) since these planets may be tidally locked, and in this case, temperature dispersion is entirely dependent on the atmosphere and/or oceans. Proxima d was presumed to have a thin or nonexistent atmosphere ($\varepsilon = 0$) and thus minimal heat distribution ($f = 0.5$) due to its very low mass and high incident stellar flux. TRAPPIST-1 d was assumed to have a dense Venus-like atmosphere and albedo. TRAPPIST-1 b (Greene et al., 2023) and c (Zieba et al., 2023) had their surface temperatures recently estimated by
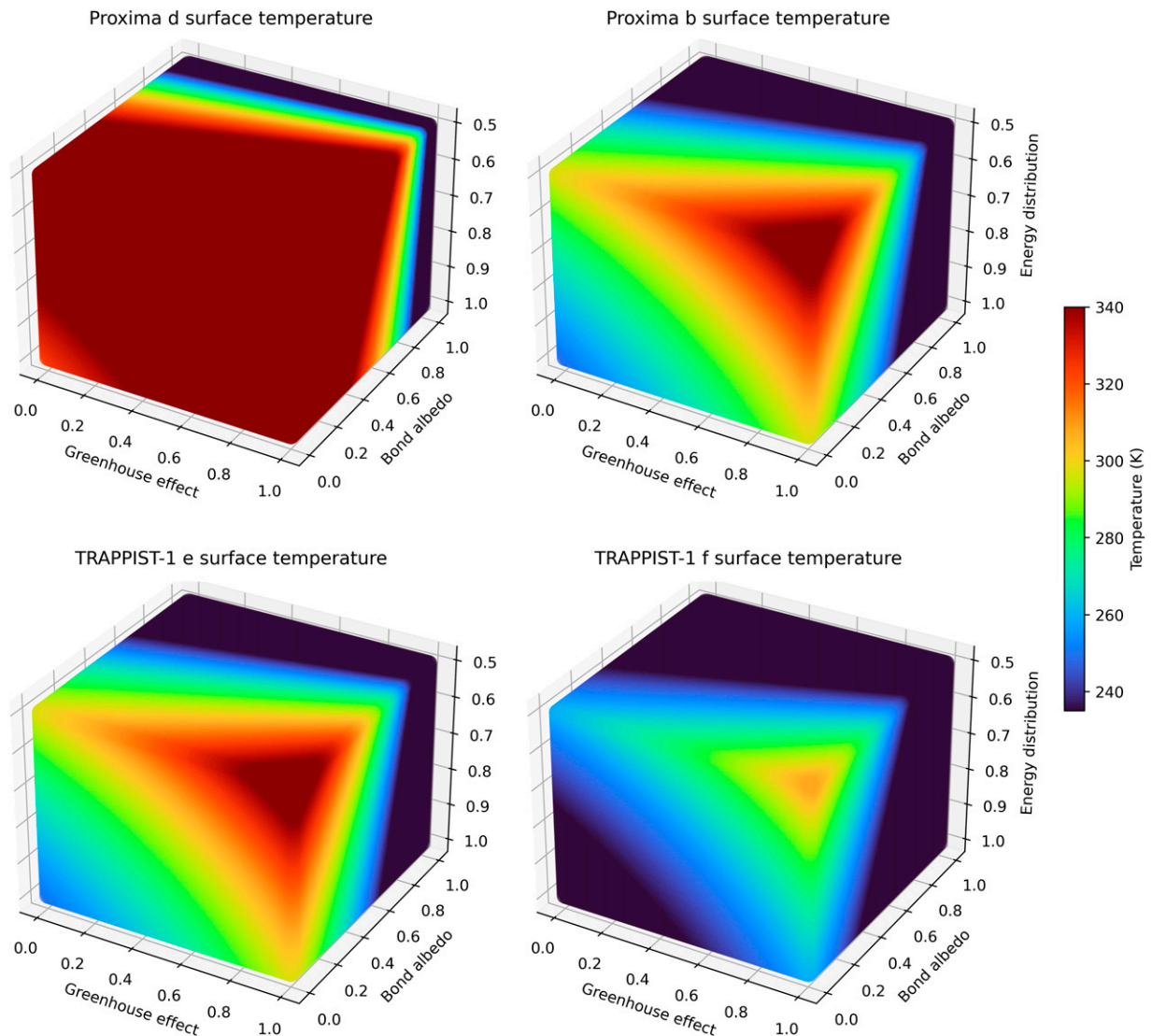
FIG. 4. Calculated dayside surface temperature matrices for some of the studied planets. Temperatures are presented in Kelvin. $N = 1$ was considered since it is not expected that any of these planets have a very thick atmosphere.

TABLE 2. MODEL RESULTS FOR THE STUDIED EXOPLANETS COMPARED WITH THE SOLAR SYSTEMS' ROCKY PLANETS

Planet	A_B	ε	N	f	T_d (calculated) (K)	T_d (measured) (K)
Mercury	0.088	0	1	0.5	520	440–700
Venus	0.77	1	56	1	738	737
Earth	0.306	0.78	1	1	288	288
Mars	0.250	0	1	1	210	208
Proxima b	0.3	0.8	1	0.75	278	?
Proxima d	0.3	0	1	0.5	351	?
TRAPPIST-1 b	0	0	1	0.5	473	503 ± 27
TRAPPIST-1 c	0	0	1	0.5	380	380 ± 31
TRAPPIST-1 d	0.8	1	50	1	605	?
TRAPPIST-1 e	0.3	0.8	1	0.75	279	?
TRAPPIST-1 f	0.3	0.8	1	0.75	243	?

$f = 0.5$ for mercury due to its slow rotation and lack of atmosphere, creating a large temperature gradient between the day and night sides due to the inefficient energy transfer.

measurements from the James Webb Space Telescope, and those results were compared with our model. Cells are color-coded to represent the general expected habitability of a planet with such T_d. Cells in green (273 K < T_d < 313 K) highlight ideal temperatures for supporting habitable environments on the surface. Cells in yellow (235 K < T_d < 340 K) highlight temperatures within the limits of possible habitability, and cells in red show likely uninhabitable conditions (Godolt et al., 2016). Table 2 also includes results for the solar system's planets and corresponding measurements found in the literature (Bauch et al., 2021; Williams, 2023).

3.2. Expected radiation environments

In Figure 5, each planet is plotted according to its orbital distance against the calculated TOA X-ray (or UV) flux it receives due to an average flare. Table 3 shows the estimated doses of UV and X-rays during flares and superflares (energy $\geq 10^{33}$ erg, Shibayama et al., 2013).

Bolometric flare energies are assumed as described in Section 2.2.2. For superflares on Proxima and TRAPPIST-1, the bolometric energy was taken from the literature (Howard et al., 2018), and the value for TRAPPIST-1 was generalized to be the minimum superflare energy since this star is less flare intensive (Yamashiki et al., 2019). In M dwarfs, the UV and X-ray flare output is similar, about 10% of the bolometric energy output of the flare (Howard et al., 2018; Welsh et al., 2007). For the Sun, a bolometric flare energy of 10^{32} erg was selected (Shibayama et al., 2013), as well as a superflare energy of 10^{34} erg (Shibata et al., 2013). Superflares with this energy occur on the Sun around every 800 years (Shibata et al., 2013). Although the Sun is a G dwarf, the same 10% fraction of the flare energy was assumed to be distributed in UV/X-rays. This is likely an overestimation of the UV and X-ray energy output during a solar flare (Reid et al., 2012; Yamashiki et al., 2019) but provides a general comparison with the irradiance expected on the studied
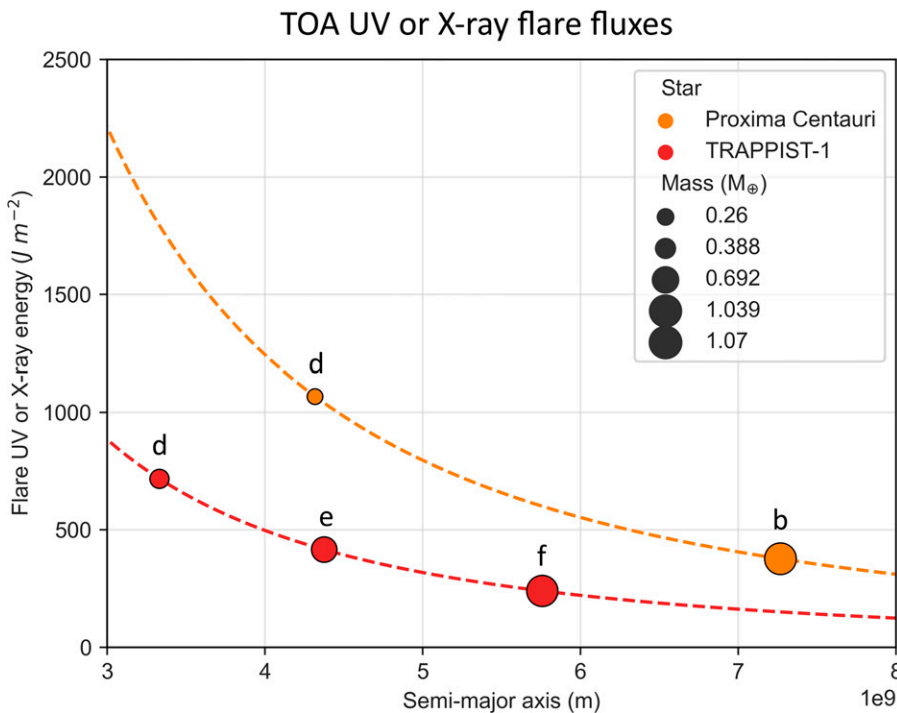
FIG. 5. TOA UV or X-ray energy received by each studied planet during a flare with average output. The masses of the planets are also illustrated, as well as their distance to their respective star. Dashed lines represent the plotting of Equation 1 with $E = 2.5 \times 10^{30}$ erg (Proxima, orange) and $E = 1.0 \times 10^{30}$ erg (TRAPPIST-1, red). TOA, top-of-atmosphere.

TABLE 3. TOP-OF-ATMOSPHERE AND SURFACE DOSES OF ULTRAVIOLET AND X-RAYS, DURING STANDARD FLARES AND SUPERFLARES ON THE STUDIED EXOPLANETS AND THE SOLAR SYSTEM'S ROCKY PLANETS, AS WELL AS LD_{90} THRESHOLDS FOR MODEL MICROORGANISMS

Flare type	Bolometric flare energy (erg)	Planet	TOA UV dose (J/m^2)	Surface UV dose (J/m^2)	TOA X-ray dose (Gy)	Surface X-ray dose (Gy)
Standard	1.00×10^{32}	Mercury	237	237	2.74×10^4	2.74×10^4
		Venus	68	—	7850	—
		Earth	36	—	4156	—
		Mars	15	8	1732	1.01×10^{-4}
	2.50×10^{31}	Proxima b	377	208	4.35×10^4	2.53×10^{-3}
		Proxima d	1067	1067	1.23×10^5	1.23×10^5
	1.00×10^{31}	TRAPPIST-1 d	717	395	8.28×10^4	4.81×10^{-3}
		TRAPPIST-1 e	416	229	4.80×10^4	2.79×10^{-3}
		TRAPPIST-1 f	240	132	2.77×10^4	1.61×10^{-3}
Superflare	1.00×10^{34}	Mercury	2.37×10^4	2.37×10^4	2.74×10^6	2.74×10^6
		Venus	6802	—	7.85×10^6	—
		Earth	3556	—	4.11×10^5	—
		Mars	1531	843	1.77×10^5	1.03×10^{-2}
	3.16×10^{33}	Proxima b	4.76×10^4	2.62×10^4	5.50×10^6	0.319
		Proxima d	1.35×10^5	1.35×10^5	1.56×10^7	1.56×10^7
	1.00×10^{33}	TRAPPIST-1 d	7.17×10^4	3.95×10^4	8.28×10^6	0.481
		TRAPPIST-1 e	4.16×10^4	2.29×10^4	4.80×10^6	0.279
		TRAPPIST-1 f	2.40×10^4	1.32×10^4	2.77×10^6	0.161

A Mars-like atmosphere with maximum transmittance was assumed to estimate the surface doses, except for Proxima d. Cells in green contain values below the LD_{90} of *Escherichia coli*, *Aspergillus niger*, and *Deinococcus radiodurans*; cells in yellow have values below the LD_{90} of only *A. niger* and *D. radiodurans*; orange cells are only below one LD_{90} (*A. niger* or *D. radiodurans*); and red cells are above all LD_{90}'s.

TOA, top-of-atmosphere; UV, ultraviolet.

exoplanets. Using Mars' atmosphere as a model, the surface doses were calculated using the modeled transmittance curves (Figs. 2 and 3), and these are shown in Table 3. Cells are colored according to the dose being above or below LD_{90} (D_{10}) values. Note that these LD_{90} values refer to more harmful UV-C irradiation, not the whole UV spectrum. Therefore, these represent a conservative estimate of the dose until a 90% reduction in population is observed.

As Table 3 emphasizes, a single flare event could sterilize the surface of mesophilic organisms, and mainly UV-hardy, spore-forming organisms such as *A. niger* would survive. Even in the presence of a Mars-like atmosphere, surface doses remain too high for mesophilic survival. Furthermore, a superflare might eliminate most, if not all, organisms on the surface due to the extremely high UV flux. However, atmospheric UV transmittance depends on many factors, including photon incidence angle and the presence of dust or hazes. For instance, Proxima b is expected to have a high superflare UV dose, reaching a surface dose of 2.62×10^4 J/m^2 with maximum transmittance and 9127 J/m^2 corresponding to UV-C. But in areas of intermediate transmittance (Fig. 3), the UV-C dose would be 1570 J/m^2, an elevated but survivable value, at least for *A. niger*, as shown in the next section. Moreover, for minimum transmittance, the superflare UV-C dose on Proxima b could be as low as 265 J/m^2, which is under the LD_{90} of *A. niger* and *D. radiodurans* as well as many other UV-tolerant organisms. On the planet with the weakest superflare irradiance, TRAPPIST-1 f, with maximum attenuation, UV-C doses only reach 134 J/m^2. Therefore, under certain conditions, even some superflares may not sterilize exoplanet surfaces of mesophilic microorganisms. For

standard flares, although a minimal atmospheric attenuation scenario leads to total UV doses >100 J/m^2 in all exoplanets of this study, limiting the survival of mesophiles like *E. coli*, maximal attenuation would reduce the doses of total UV to ≤53 J/m^2, and as low as 12 J/m^2, which would not create a significant hazard to most microorganisms. The subsurface environment could also shield cells from UV at even shallow depths since UV-C soil penetration depth is ≤0.11 mm (Ciani et al., 2005).

In the presence of an atmosphere, the same risk is not seen for X-rays, which, even for the strongest flares, generate low doses that do not pose a threat to microorganisms on the surface. Nonetheless, with no atmosphere present, the X-ray surface dose would be extremely elevated, potentially sterilizing the ground. In this scenario, some microorganisms could survive by living in the subsurface, where the dose very rapidly decreases at relatively shallow depths. For a superflare on Proxima b, the surface X-ray dose without an atmosphere is 5.50×10^6 Gy, but the dose below a 0.15 mm thick layer of soil (866 Gy) or water (9550 Gy) would be lower than the LD_{90} of extreme radiotolerant organisms like *D. radiodurans* (Fig. 6). Moreover, at depths over 1 mm of soil or 10 mm of water, most organisms—even mesophiles like *E. coli*—could survive, meaning that subsurface and underwater environments would shield microorganisms from X-ray damage.

For an Earth-like atmosphere, the opacity to X-rays is essentially 100%, and surface doses are negligible. There would also be increased UV protection, with UV-C being mostly eliminated and UV-B drastically reduced (Segura et al., 2010).
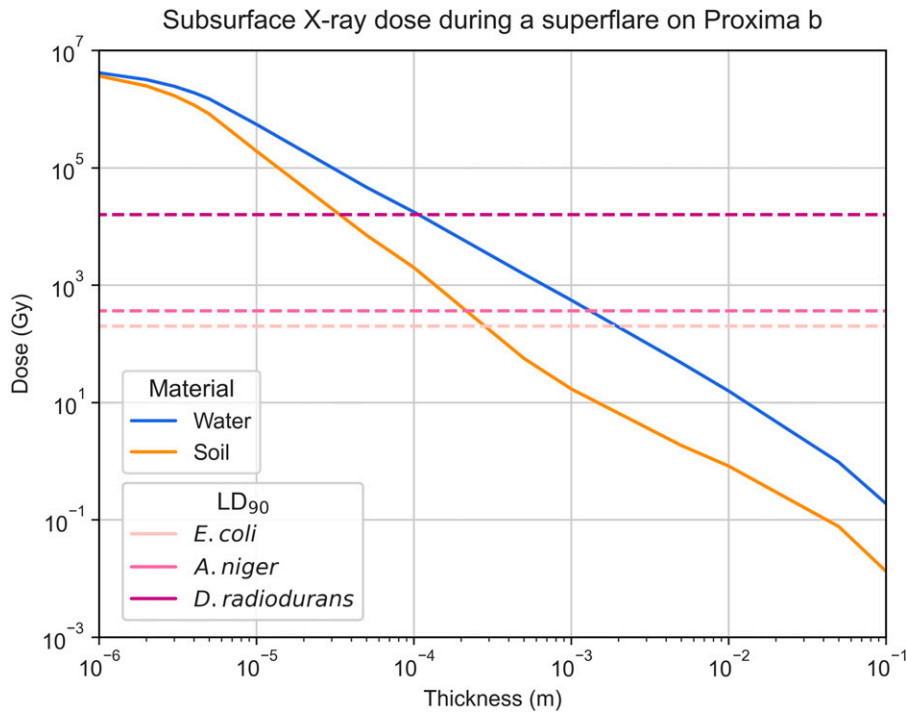
FIG. 6. Estimated subsurface X-ray absorbed dose throughout a thin layer of soil (orange) or water (blue). Water has a lower capacity for attenuating these high-energy photons, leading to the need for a thicker layer to reduce the same dose when compared to soil. Dashed lines represent the LD_{90} values for *Escherichia coli*, *Aspergillus niger*, and *Deinococcus radiodurans*.

3.3. Survival and germination of A. niger spores to flare UV and X-ray irradiation and the multifunctional role of melanin

Initial assays were performed to evaluate the outgrowth of wild-type and mutant *A. niger* spores after X-ray irradiation (Fig. 7) considering a maximum dose of 1000 Gy, rounded up from the estimated Proxima b dose below 0.15 mm of soil (or 0.7 mm water) of 866 Gy mentioned in the previous section. Significant germination was observed in the strains with an irradiation of 100 Gy, with the wild type achieving around 1.2 SESA (a growth index calculated by the oCello-Scope to track fungal germination) and the mutant about 0.9. This is still a reduction when compared to the control, both for the wild-type (SESA $\approx$ 1.4, M-W, $p < 0.00001$) and the mutant (SESA $\approx$ 1.2, M-W, $p = 0.00008$) spores. To receive

this dose, the spores would need shielding of 0.4 mm of soil or 3 mm of water. At 500 Gy (0.2 mm soil, 1 mm water), some germination of the wild type was observed (SESA $\approx$ 0.4). This is significantly more than the mutant (M-W, $p = 0.005$). At the largest dose of 1000 Gy, little germination (<0.3 SESA) was seen in any strain.

To test the protective efficiency of a solid melanin layer versus the melanin-rich solution produced by the growth of OS4.3, wild-type and mutant spores of the strain were irradiated with 1000 Gy of X-rays while suspended in either a standard saline solution or the filtered melanin-rich solution. Three samples suspended in 0.9% NaCl were under a thin solid melanin film. As seen in Figure 8, for both the wild-type and the mutant (K-W, $p < 0.00001$), there was greater
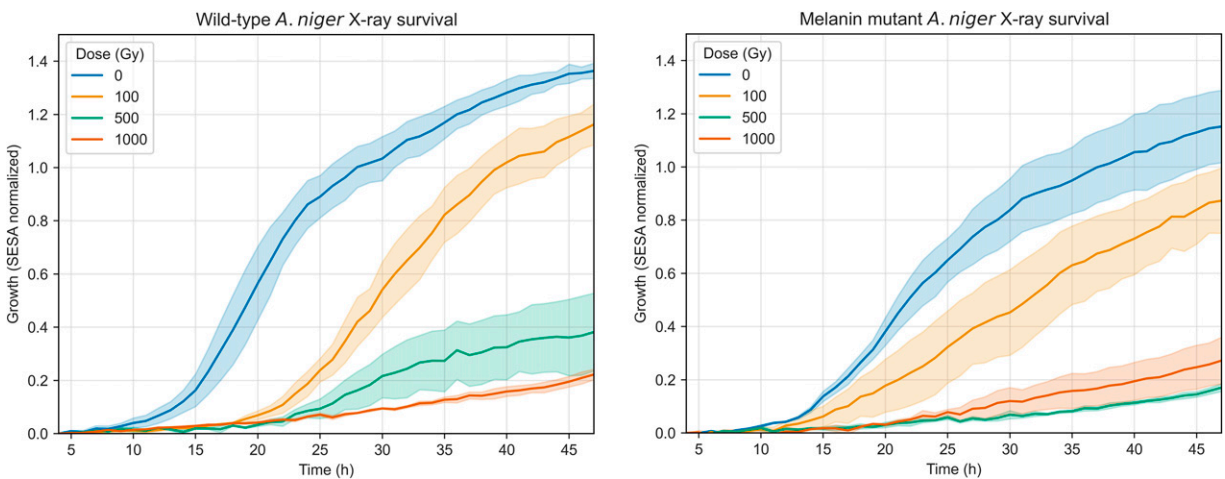
FIG. 7. Spore germination of *A. niger* wild-type (left) and mutant (right) strains after X-ray irradiation, measured through the SESA fungi algorithm of the oCelloScope. Uncertainty bands represent the standard error over the replicates ($n = 3$). The normalization was done at $t = 4$ h as detailed in the Methods section.
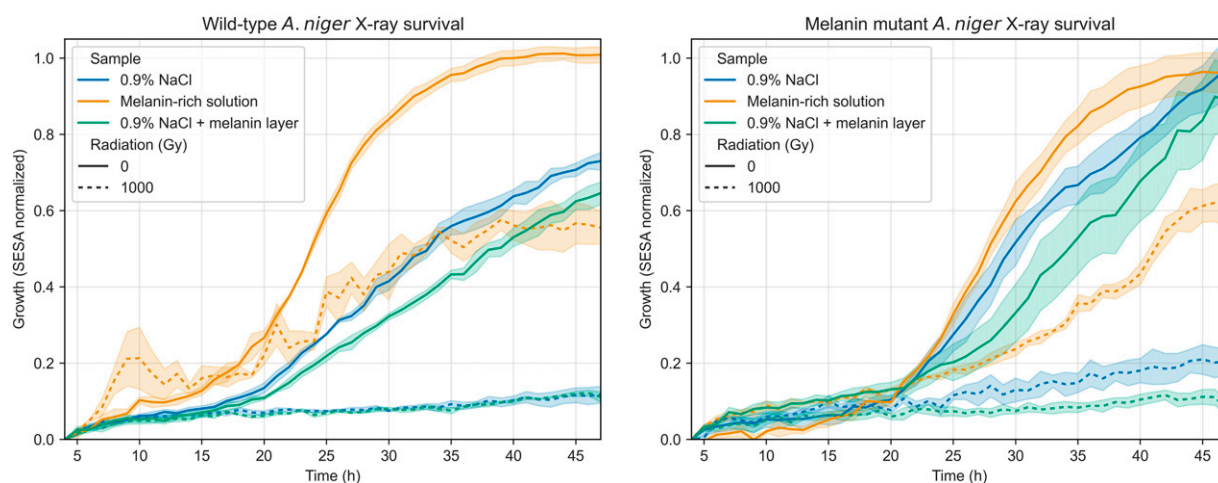
FIG. 8. Spore germination of *A. niger* wild-type (left) and mutant (right) strains in two different solutions. The protective effect of a solid melanin layer was also tested on three samples in saline solution. Data presented show irradiated (1000 Gy X-rays, dashed lines) and control samples (nonirradiated, solid lines).

germination for irradiated spores suspended in the melanin-rich solution, whereas no shielding effect was seen for the solid melanin film, both on the wild-type and mutant. The melanin-rich nonirradiated controls grew better than their saline solution counterparts in the wild-type (M-W, $p < 0.00001$), but not significantly so for the mutant (M-W, $p = 0.52$), although a tendency for faster germination in melanin was observed. Figure 9 shows images of samples in 0.9% NaCl and the melanin solution at 5 and 48 h after inoculation in MM.

After these tests, additional experiments were performed to further characterize the beneficial effects of suspension in a melanin-rich solution for both UV-C and X-ray irradiation shielding and spore recovery after irradiation. Survival assays showed that melanin-deficient *A. niger* MA93.1 spores survived 5000 J/m^2 of UV-C (254 nm) if suspended in a control supernatant or in a melanin-rich supernatant (Fig. 10). Survival was higher when melanin was present (*t* test, $p = 0.006$), since an average of 44% of spores in melanin survived the highest dose, whereas 2.7% survived in the control supernatant. Survival fraction change was negligible between 1000 and 5000 J/m^2, which was not the case for the control

supernatant (with fungal extracellular compounds but without melanin). In contrast, spores suspended in saline solution were significantly more susceptible to UV-C, even at 1000 J/m^2 (*t* test, $p = 0.01$), and less than 1% survived until 2500 J/m^2. No survival was observed at the highest tested dose.

Spores of the melanin-deficient strain irradiated with X-rays showed a similar dose–response pattern, with only the spores suspended in the melanin solution surviving a dose of 1000 Gy, although the inactivation fraction was >99%. Control samples showed improved survival at 500 Gy when compared to 0.9% NaCl samples (*t* test, $p = 0.03$), though in both cases no spores survived higher doses ($\geq$1000 Gy). No samples survived a 2000 Gy irradiation.

Figure 11 suggests that spores in melanin solutions germinated faster and more efficiently than those in saline solution or a control supernatant, both for irradiated and nonirradiated samples, which indicates that extracellular melanin could be a spore germination trigger.

4. Discussion

4.1. Models of (exo)planetary surface temperature and radiation environment

We developed a robust but streamlined 0D model to estimate a planet's dayside surface temperature. Complex models, like general circulation models, although potentially more accurate, require a greater amount and precision of information, which is largely unknown for exoplanets. Equation 1 is not intended to be an alternative to 1D–3D models but rather an efficient tool when not enough information is present and rapid, general estimations under various conditions are intended. This allows astrobiologists to construct an overview of different possibilities to then plan experiments for simulated exoplanet environments.

Furthermore, we developed versatile models to estimate the flare TOA, surface and subsurface doses of UV and X-rays on exoplanets, and their effect on model microorganisms, by using the martian atmosphere as a model. The atmospheric attenuation model for X-rays does not account for various physical processes, such as photon interactions, secondary production,
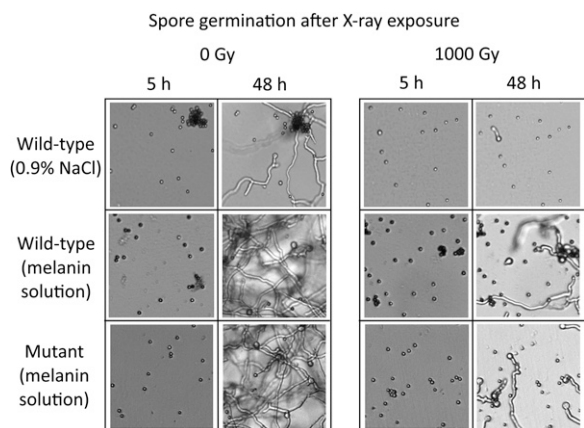
FIG. 9. Images from the germination of *A. niger* spores, in a saline solution (0.9% NaCl), or a filtered supernatant containing solubilized pyomelanin. Control and irradiated (1000 Gy of X-rays) samples of the wild-type and mutant strains are shown.
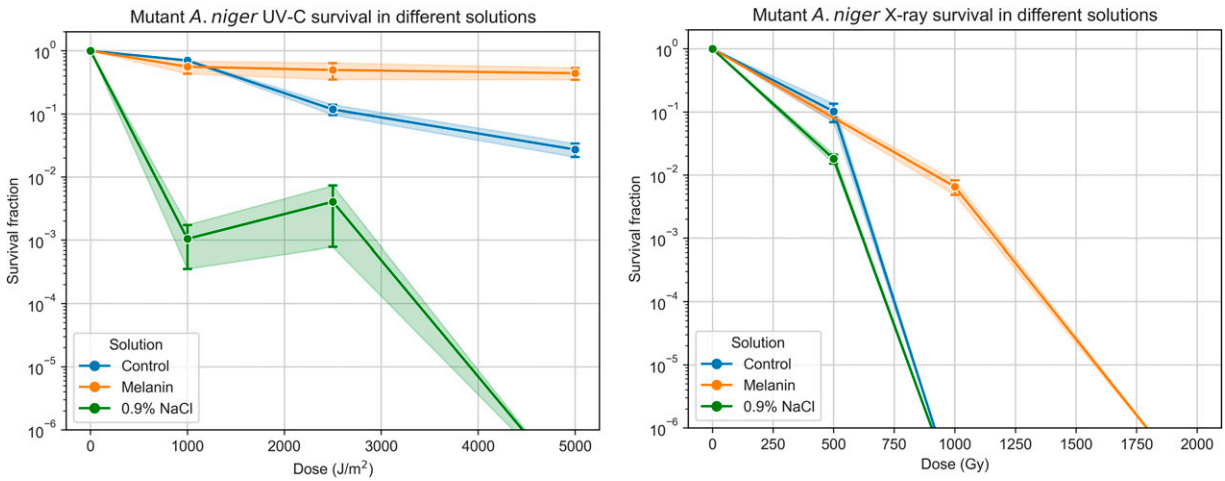
FIG. 10. Survival fractions of *A. niger* MA93.1 spores when exposed to UV-C (left) and X-ray radiation (right) in three distinct solutions: a 0.9% NaCl solution, a melanin-free supernatant ("Melanin"), and an identical but melanin-rich supernatant ("Control").

and charge-particle equilibrium, and only vertical column density is factored in, neglecting horizontal attenuation. When modeling UV attenuation, the equations used were based on generalization of the martian atmospheric transmittance under three sets of conditions and thus do not adequately characterize all possible combinations of atmospheric traits. Nonetheless, the developed equations are useful to inform microbiological experiments for exoplanet flare irradiation studies.

4.2. Are Proxima b and TRAPPIST-1 e good candidates for (sub)surface habitability?

Estimated dayside temperatures for Proxima b and d, and TRAPPIST-1 d, e, and f are in line with the values estimated from more complex models (Boutle et al., 2017; Lincowski et al., 2018; Sergeev et al., 2020; Turbet et al., 2016; Wolf, 2017; Wunderlich et al., 2020). According to our results, Proxima b and TRAPPIST-1 e are good candidates to

have potential temperature environments, enhancing their habitability.

Planetary radiation doses depend on stellar flare energy and planetary traits (orbit and atmosphere). If unattenuated, X-rays from flares would most likely sterilize the surface of all studied exoplanets. However, microorganisms suited to survive under the surface would be unaffected by most exogenous radiation sources under a few millimeters of soil or water.

4.3. Melanin-rich solutions increase the survival and germination of A. niger spores

The experiments performed in this study corroborate the multifunctional purpose of melanin since *A. niger* MA93.1 spores germinated faster and more efficiently in a melanin-rich extract when compared to the two control solutions (Fig. 9). Nonirradiated spores in both control solutions
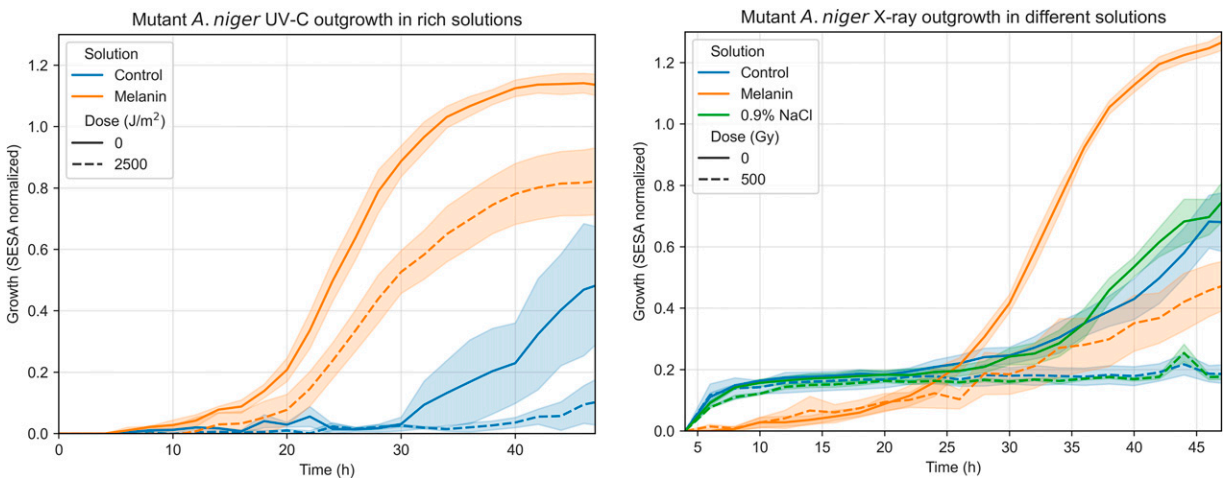
FIG. 11. Left—Measured germination of *A. niger* melanin mutant (MA93.1) in two different supernatant solutions, one melanin-rich ("Melanin") and another free of melanin ("Control"). Data presented show irradiated (2500 J/m² UV-C, dashed lines) and control samples (nonirradiated, solid lines). Right—Measured germination of *A. niger* melanin mutant (MA93.1) in three different solutions. Data presented show irradiated (500 Gy X-rays, dashed lines) and control samples (nonirradiated, solid lines).

showed similar outgrowth capability (Fig. 8). Both untreated and irradiated spores in the melanin-rich solution showed greater germination capacity than the controls, including the formation of more complex hyphal networks (Fig. 9). Outgrowth capacity is connected not only to the survival rate but also to the rate of DNA repair. The time required for cells or spores to accumulate a given dose of ionizing radiation depends on the radiation's type, fluence, and intensity and is not instantaneous. Faster germination indicates either less DNA damage or faster DNA repair since *Aspergillus* spores that detect altered DNA inhibit the germination process until repair is complete (Harris and Kraus, 1998; Ye et al., 1997). The damage induced will affect cellular pathways and division mainly during the S and G2 phases, where DNA replication and repair occur. High radiation doses on short timeframes can delay or arrest the cell cycle at G2/M checkpoints due to unrepairable double-strand breaks. In *A. niger* spores, once the accumulated damage exceeds critical levels, a reactivation of an active metabolic state is inhibited.

For irradiated spores, a clear increase in survival was seen in samples containing melanin (Fig. 10). For UV-C, nearly half of the spores survived a 5000 J/m^2 dose, comparable to a superflare on TRAPPIST-1 f with minimum atmospheric attenuation (4602 J/m^2 of UV-C), which indicates that a significant fraction of spores in these conditions could survive superflares on the exoplanets more likely to be habitable—Proxima b (9127 J/m^2) and TRAPPIST-1 e (7976 J/m^2)—even with minimal atmospheric shielding. Finally, for X-rays, spores in the control solutions survived only up to 500 Gy, while samples in the melanin-rich solution showed survival up to 1000 Gy, as well as increased germination capacity in all scenarios.

The functional diversity of microbial melanins is notable, as they have been associated with a variety of roles (Cordero and Casadevall, 2017). However, no prior research had found a correlation between solubilized melanin and spore development efficiency. To explain our results, we suggest that the effect of the presence of melanin is twofold. First, for irradiated samples, it serves an attenuation purpose, protecting the spores from direct damage from incoming radiation. Second, the presence of melanin in the medium may be advantageous in cellular processes that could promote the upkeep of a high spore viability and growth efficiency, for example, through reactive oxygen species scavenging or by triggering quorum sensing pathways related to germination. Although the production of melanin is regulated by quorum sensing in fungal species (Albuquerque et al., 2013; Homer et al., 2016), no studies have identified melanin as participating as an inducer. Finally, melanin could have functions that directly impact spore germination, hyphal morphogenesis, and growth rate, as demonstrated in *A. niger* (Cortesão et al., 2022) and other fungal species (*e.g.*, Yu et al., 2015). In any case, follow-up experiments are required to better explain the results obtained in this work, including testing the wild-type strain and performing detailed biochemical characterization of the melanin-rich solution.

These findings highlight the importance of expanding microbiological experiments to incorporate potential exoplanet-like conditions and thus help explore the boundaries of life beyond Earth, Mars, and the icy moons of the solar system. Our work serves as a foundation for future studies to further investigate the adaptability and survival mechanisms of microorganisms under extrasolar extreme environments. Future studies could build on this approach by exploring different microbial species, environmental conditions, transcriptomic or proteomic adaptations, and possible new biosignatures to better understand the potential for life across the galaxy.

5. Conclusion

Overall, the work developed during this study highlights the advantages of applying an interdisciplinary approach to astrobiology and exoplanet science. The lack of detailed information about exoplanet surfaces has led astrobiologists to resort to useful, though generalized, measures of habitability, such as the equilibrium temperature and the Goldilocks zone. As we showed during this work, a combined approach that leverages astrophysical modeling and observational extrapolation of exoplanet conditions (*e.g.*, temperature, radiation environment) with microbiological experiments may allow astrobiologists to construct hypothetical, yet more realistic, model environments on which to test microbial survival and growth. Furthermore, results from this work showed how *A. niger*, like other extremotolerant and extremophilic organisms, would be able to survive harsh radiation conditions on the surface of some M dwarf exoplanets. Additionally, melanin-rich solutions were shown to be highly beneficial to the survival and germination of *A. niger* spores, particularly when treated with high doses of UV and X-ray radiation. These results offer an insight into how life forms may endure harmful events and conditions prevalent on exoplanets, and how melanin may have had a role in the origin and evolution of life on Earth and perhaps on other worlds.

Authors' Contributions

A.M.: Conceptualization, data curation, formal analysis, investigation, methodology, project administration, visualization, writing—original draft, and writing—review and editing. S.K.: Methodology, resources, validation, and writing—review and editing. D.M.: Methodology, validation, and writing—review and editing. N.S.: Supervision and writing—review and editing. M.C.: Conceptualization, methodology, project administration, resources, supervision, and writing—review and editing.

Author Disclosure Statement

The authors declare no competing interests.

Supplementary Material

Supplementary Data S1

Supplementary Figure S1
Supplementary Figure S2

References

Agol E, Dorn C, Grimm SL, et al. Refining the transit-timing and photometric analysis of TRAPPIST-1: Masses, radii, densities, dynamics, and ephemerides. *Planet Sci J* 2021; 2(1):1; doi: 10.3847/PSJ/abd022

Albuquerque P, Nicola AM, Nieves E, et al. Quorum sensing-mediated, cell density-dependent regulation of growth and virulence in cryptococcus neoformans. *mBio* 2013;5(1): e00986–e00913; doi: 10.1128/mbio.00986-13

Anglada-Escudé G, Amado PJ, Barnes J, et al. A terrestrial planet candidate in a temperate orbit around Proxima Centauri. *Nature* 2016;536(7617):437–440; doi: 10.1038/nature19106

Bauch KE, Hiesinger H, Greenhagen BT, et al. Estimation of surface temperatures on Mercury in preparation of the MERTIS experiment onboard BepiColombo. *Icarus* 2021;354:114083; doi: 10.1016/j.icarus.2020.114083

Berger MJ. XCOM: Photon cross sections database. *Physical Measurement Laboratory* 1998;8:3587. https://physics.nist .gov/PhysRefData/Xcom/html/xcom1.html

Boutle IA, Mayne NJ, Drummond B, et al. Exploring the climate of Proxima B with the Met Office Unified Model. *A&A* 2017;601:A120; doi: 10.1051/0004-6361/201630020

Brock TD, Madigan MT, Martinko JM, et al. *Brock biology of microorganisms*. Upper Saddle River (NJ): Prentice-Hall, 2003.

Bucheli-Witschel M, Bassin C, Egli T. UV-C inactivation in Escherichia coli is affected by growth conditions preceding irradiation, in particular by the specific growth rate. *J Appl Microbiol* 2010; 109(5):1733–1744; doi: 10.1111/j.1365-2672.2010.04802.x

Cairns TC, Nai C, Meyer V. How a fungus shapes biotechnology: 100 years of Aspergillus niger research. *Fungal Biol Biotechnol* 2018;5(1):13; doi: 10.1186/s40694-018-0054-5

Cannon KM, Britt DT, Smith TM, et al. Mars global simulant MGS-1: A Rocknest-based open standard for basaltic martian regolith simulants. *Icarus* 2019;317:470–478; doi: 10.1016/j .icarus.2018.08.019

Ciani A, Goss KU, Schwarzenbach R. Light penetration in soil and particulate minerals. *European J Soil Science* 2005; 56(5):561–574; doi: 10.1111/j.1365-2389.2005.00688.x

Cockell CS, Catling DC, Davis WL, et al. The ultraviolet environment of Mars: Biological implications past, present, and future. *Icarus* 2000;146(2):343–359; doi: 10.1006/icar.2000.6393

Coelho LF, Madden J, Kaltenegger L, et al. Color catalogue of life in ice: Surface biosignatures on icy worlds. *Astrobiology* 2022;22(3):313–321; doi: 10.1089/ast.2021.0008

Cordero RJ, Casadevall A. Functions of fungal melanin beyond virulence. *Fungal Biol Rev* 2017;31(2):99–112; doi: 10.1016/ j.fbr.2016.12.003

Cortesão M, de Haas A, Unterbusch R, et al. Aspergillus niger spores are highly resistant to space radiation. *Front Microbiol* 2020;11:560; doi: 10.3389/fmicb.2020.00560

Cortesão M, Holland G, Schütze T, et al. Colony growth and biofilm formation of Aspergillus niger under simulated microgravity. *Front Microbiol* 2022;13:975763; doi: 10.3389/fmicb .2022.975763

Cortesão M, Siems K, Koch S, et al. MARSBOx: Fungal and bacterial endurance from a balloon-flown analog mission in the stratosphere. *Front Microbiol* 2021;12:601713; doi: 10 .3389/fmicb.2021.601713

de Vera J-P, Alawi M, Backhaus T, et al. Limits of life and the habitability of mars: The ESA space experiment BIOMEX on the ISS. *Astrobiology* 2019;19(2):145–157; doi: 10.1089/ast .2018.1897

d'Ischia M, Manini P, Martins Z, et al. Insoluble organic matter in chondrites: Archetypal melanin-like PAH-based multifunctionality at the origin of life? *Phys Life Rev* 2021;37:65–93; doi: 10.1016/j.plrev.2021.03.002

Faria JP, Suárez Mascareño A, Figueira P, et al. A candidate short-period sub-Earth orbiting Proxima Centauri. *A&A* 2022;658:A115; doi: 10.1051/0004-6361/202142337

Gascón J, Oubiña A, Pérez-Lezaun A, et al. Sensitivity of selected bacterial species to UV radiation. *Curr Microbiol* 1995;30(3):177–182; doi: 10.1007/BF00296205

Godolt M, Grenfell JL, Kitzmann D, et al. Assessing the habitability of planets with Earth-like atmospheres with 1D and 3D climate modeling. *A&A* 2016;592:A36; doi: 10.1051/ 0004-6361/201628413

Greene TP, Bell TJ, Ducrot E, et al. Thermal emission from the earth-sized exoplanet TRAPPIST-1 b using JWST. *Nature* 2023;618(7963):39–42; doi: 10.1038/s41586-023-05951-7

Harris SD, Kraus PR. Regulation of septum formation in Aspergillus nidulans by a DNA damage checkpoint pathway. *Genetics* 1998;148(3):1055–1067; doi: 10.1093/ genetics/148.3.1055

Homer CM, Summers DK, Goranov AI, et al. Intracellular action of a secreted peptide required for fungal virulence. *Cell Host Microbe* 2016;19(6):849–864; doi: 10.1016/j.chom.2016.05.001

Howard WS, Tilley MA, Corbett H, et al. The first naked-eye superflare detected from proxima centauri. *The Astrophysical Journal* 2018;860(2); doi: 10.3847/2041-8213/aacaf3

Hubbell J, Stephen S. *Tables of X-ray mass attenuation coefficients and mass energy-absorption coefficients 1 keV to 20 MeV for Elements Z = 1 to 92 and 48 additional substances of dosimetric interest*. U.S. National Institute of Standards and Technology (NIST): 1995; No. PB-95-220539/XAB; NISTIR-225632.

Inglis AR. *Quasi-periodic pulsations in solar flares*. Department of Physics, University of Warwick: 2009.

Jacob DJ. *Introduction to Atmospheric Chemistry*. Princeton University Press; 1999.

Jørgensen TR, Park J, Arentshorst M, et al. The molecular and genetic basis of conidial pigmentation in Aspergillus niger. *Fungal Genet Biol* 2011;48(5):544–553; doi: 10.1016/j.fgb .2011.01.005

Kasting JF, Whitmire DP, Reynolds RT. Habitable zones around main sequence stars. *Icarus* 1993;101(1):108–128; doi: 10.1006/icar.1993.1010

Koch SM, Pohl C, Siontas O, et al. Aspergillus niger as a cell factory for the production of pyomelanin, a molecule with UV-C radiation shielding activity. *Front Microbiol* 2023;14: 1233740; doi: 10.3389/fmicb.2023.1233740

Krissansen-Totton J, Fortney JJ. Predictions for observable atmospheres of trappist-1 planets from a fully coupled atmosphere–interior evolution model. *ApJ* 2022;933(1):115; doi: 10.3847/1538-4357/ac69cb

Kump LR, Kasting JF, Crane RG. *The Earth System*. Pearson New International: 2014.

Lincowski AP, Meadows VS, Crisp D, et al. Evolved climates and observational discriminants for the TRAPPIST-1 planetary system. *ApJ* 2018;867(1):76; doi: 10.3847/1538-4357/aae36a

Liu WS. Comparison of the greenhouse effect between Earth and Venus using multiple atmospheric layer models. *E3S Web Conf* 2020;167:e04002.

Maas AJ, Ilin E, Oshagh M, et al. Lower-than-expected flare temperatures for TRAPPIST-1. *A&A* 2022;668:A111; doi: 10.1051/0004-6361/202243869

Madhusudhan N, Piette AAA, Constantinou S. Habitability and biosignatures of hycean worlds. *ApJ* 2021;918(1):1; doi: 10.3847/1538-4357/abfd9c

Maggio A. Non-thermal hard X-ray emission from stellar coronae. *Memorie Della Società Astronomica Italiana* 2008;79:186.

Malik K, Tokkas J, Goyal SL. Microbial pigments: A review. *International Journal of Microbial Resource Technology* 2012;1(4):361–365.

Moreira RG, Puerta-Gomez AF, Kim J, et al. Factors affecting radiation D-values (D_{10}) of an Escherichia coli cocktail and Salmonella Typhimurium LT2 inoculated in fresh produce. *Journal of Food Science* 2012;77(4):E104–E111; doi: 10.1111/j.1750-3841.2011.02603.x

Nimmo F, Pappalardo RT. Ocean worlds in the outer solar system. *JGR Planets* 2016;121(8):1378–1399; doi: 10.1002/2016JE005081

Onofri S, de Vera J-P, Zucconi L, et al. Survival of antarctic cryptoendolithic fungi in simulated martian conditions on board the international space station. *Astrobiology* 2015;15(12):1052–1059; doi: 10.1089/ast.2015.1324

Pacelli C, Cassaro A, Aureli L, et al. The responses of the black fungus cryomyces antarcticus to high doses of accelerated helium ions radiation within martian regolith simulants and their relevance for mars. *Life (Basel)* 2020;10(8); doi: 10.3390/life10080130

Palle E, Biazzo K, Bolmont E, et al. Ground-breaking Exoplanet Science with the ANDES spectrograph at the ELT. *arXiv* 2023.

Pavlenko Y, Suárez Mascareño A, Rebolo R, et al. Flare activity and photospheric analysis of Proxima Centauri. *A&A* 2017;606:A49; doi: 10.1051/0004-6361/201730733

Quarles B, Quintana EV, Lopez E, et al. Plausible compositions of the seven TRAPPIST-1 planets using long-term dynamical simulations. *The Astrophysical Journal* 2017;842(1); doi: 10.3847/2041-8213/aa74bf

Ranjan S, Wordsworth R, Sasselov DD. The surface UV environment on planets orbiting m dwarfs: Implications for prebiotic chemistry and the need for experimental follow-up. *ApJ* 2017;843(2):110; doi: 10.3847/1538-4357/aa773e

Rauer H, Catala C, Aerts C, et al. THE PLATO 2.0 mission. *Exp Astron* 2014;38(1–2):249–330; doi: 10.1007/s10686-014-9383-4

Reid HAS, Vilmer N, Aulanier G, et al. X-ray and ultraviolet investigation into the magnetic connectivity of a solar flare. *A&A* 2012;547:A52; doi: 10.1051/0004-6361/201219562

Romsdahl J, Blachowicz A, Chiang AJ, et al. Characterization of Aspergillus niger isolated from the international space station. *mSystems* 2018;3(5):e00112-18; doi: 10.1128/mSystems.00112-18

Schwieterman EW, Cockell CS, Meadows VS. Nonphotosynthetic pigments as potential biosignatures. *Astrobiology* 2015;15(5):341–361; doi: 10.1089/ast.2014.1178

Seager S. Exoplanet habitability. *Science* 2013;340(6132):577–581; doi: 10.1126/science.1232226

Seager S. *Exoplanets*. University of Arizona Press: 2011.

Segura A, Walkowicz LM, Meadows V, et al. The effect of a strong stellar flare on the atmospheric chemistry of an earth-like planet orbiting an M dwarf. *Astrobiology* 2010;10(7):751–771; doi: 10.1089/ast.2009.0376

Sergeev DE, Lambert FH, Mayne NJ, et al. Atmospheric convection plays a key role in the climate of tidally locked terrestrial exoplanets: Insights from high-resolution simulations. *ApJ* 2020;894(2):84; doi: 10.3847/1538-4357/ab8882

Shibata K, Isobe H, Hillier A, et al. Can superflares occur on our sun? *Publications of the Astronomical Society of Japan* 2013;65(3):49; doi: 10.1093/pasj/65.3.49

Shibayama T, Maehara H, Notsu S, et al. Superflares on solar-type stars observed with Kepler. I. Statistical properties of superflares. *ApJS* 2013;209(1):5.

Slade D, Radman M. Oxidative stress resistance in deinococcus radiodurans. *Microbiol Mol Biol Rev* 2011;75(1):133–191; doi: 10.1128/mmbr.00015-10

Smith DS, Scalo J. Solar X-ray flare hazards on the surface of Mars. *Planetary and Space Science* 2007;55(4):517–527; doi: 10.1016/j.pss.2006.10.001

Suárez Mascareño A, Faria JP, Figueira P, et al. Revisiting proxima with ESPRESSO. *A&A* 2020;639:A77.

Tilley MA, Segura A, Meadows V, et al. Modeling repeated M dwarf flaring at an earth-like planet in the habitable zone: Atmospheric effects for an unmagnetized planet. *Astrobiology* 2019;19(1):64–86; doi: 10.1089/ast.2017.1794

Turbet M, Leconte J, Selsis F, et al. The habitability of Proxima Centauri b. *A&A* 2016;596:A112; doi: 10.1051/0004-6361/201629577

Welsh BY, Wheatley JM, Seibert M, et al. The detection of M dwarf UV flare events in the GALEX data archives. *Astrophys J (Suppl S)* 2007;173(2):673–681.

Williams DR. Planetary Fact Sheet. 2023. Available from: https://nssdc.gsfc.nasa.gov/planetary/factsheet/ [Last accessed: June, 2023].

Williams DR. Sun Fact Sheet. 2022. Available from: https://nssdc.gsfc.nasa.gov/planetary/factsheet/sunfact.html [Last accessed: June, 2023].

Wolf ET. Assessing the habitability of the TRAPPIST-1 system using a 3D climate model. *ApJL* 2017;839(1):L1; doi: 10.3847/2041-8213/aa693a

Wunderlich F, Scheucher M, Godolt M, et al. Distinguishing between Wet and Dry Atmospheres of TRAPPIST-1 e and f. *ApJ* 2020;901(2):126; doi: 10.3847/1538-4357/aba59c

Xu X, Cao R, Li K, et al. The protective role and mechanism of melanin for Aspergillus niger and Aspergillus flavus against chlorine-based disinfectants. *Water Res* 2022;223:119039; doi: 10.1016/j.watres.2022.119039

Yamashiki YA, Maehara H, Airapetian V, et al. Impact of stellar superflares on planetary habitability. *ApJ* 2019;881(2):114; doi: 10.3847/1538-4357/ab2a71

Ye XS, Fincher RR, Tang A, et al. The G2/M DNA damage checkpoint inhibits mitosis through Tyr15 phosphorylation of p34cdc2 in Aspergillus nidulans. *Embo J* 1997;16(1):182–192; doi: 10.1093/emboj/16.1.182

Yu X, Huo L, Liu H, et al. Melanin is required for the formation of the multi-cellular conidia in the endophytic fungus Pestalotiopsis microspora. *Microbiol Res* 2015;179:1–11; doi: 10.1016/j.micres.2015.06.004

Zieba S, Kreidberg L, Ducrot E, et al. No thick carbon dioxide atmosphere on the rocky exoplanet TRAPPIST-1 c. *Nature* 2023;620(7975):746–749; doi: 10.1038/s41586-023-06232-z

Address correspondence to:
Afonso Mota
Aerospace Microbiology Research Group
Institute of Aerospace Medicine
German Aerospace Center (DLR), Linder Höhe
51147 Köln
Germany

E-mail: afonsomota.papers@gmail.com

Marta Cortesão
Aerospace Microbiology Research Group
Institute of Aerospace Medicine
German Aerospace Center (DLR)
Cologne
Germany

E-mail: martacortesao.papers@gmail.com

Abbreviations Used

AU = astronomical units
CFU = colony-forming unit
CM = complete medium
Gy = gray
LD = lethal dose
MM = minimal medium
SESA = Segmentation and Extraction of Surface Area
TOA = Top-of-atmosphere
UV = ultraviolet